INFLUENCE OF AXIAL MISALIGNMENT TO A TMF DRIVEN FLOW

Kristina Koal, Silvio Tschisgale, and Jörg Stiller
Institute of Fluid Mechanics
Technische Universität Dresden
01062 Dresden, Germany
kristina.koal@tu-dresden.de
silvio.tschisgale@mailbox.tu-dresden.de
joerg.stiller@tu-dresden.de

ABSTRACT

The travelling magnetic field (short: TMF) is a commonly used alternating magnetic field, which is applied e.g. to tailor heat and mass transport during crystal growth processes. Numerical studies usually assume ideal configurations such as a perfectly adjusted magnetic field. However, an ideal setup can be hardly realized in "real processes". In the present work, we study the sensitivity of a TMF driven fluid flow within a cylindrical configuration, when a small offset is introduced between the container's axis and that one of the magnetic field. It will be shown, that already a small misalignment affects the flow seriously. Especially in supercritical regimes the mean flow as well as the turbulent structures changes considerably, whereas the variations in the laminar regime correlate approximately with the magnitude of the axes' shift.

1 INTRODUCTION

Contactless mixing of electrically conductive liquids with magnetic fields plays an important role in metallurgical processes like crystal growth or casting. During the last years, the flow topology in a closed cylinder, a typical test configuration, was investigated both experimentally and numerically for different types of single and combined magnetic fields. One configuration, which is of particular interest, is the so-called travelling magnetic field. In the laminar regime, the TMF generates a toroidal flow in the meridional directions; see e.g. [1, 2]. Further investigations in the turbulent regime confirmed this property for the mean flow and further revealed a high degree of turbulence for moderate forcing parameters [3, 4]. These studies rely on the assumption, that the cylinder filled with the liquid metal is exactly positioned in the middle of the magnetic field. However, this assumption can be rarely satisfied in industrial processes and hard to achieve even in experimental setups. In a combined experimental and numerical study [5] the sensitivity of the fluid flow was examined when the container is shifted slightly within the magnetic field as shown in Fig.1. It was shown, that even a small offset r_0 causes a strong flow reorganization in a turbulent regime. However, these studies were restricted to the mean velocities; information about turbulence characteristics was not provided. In this paper, we present a follow-up investigation to get a deeper insight. In addition, we examine a supplemental laminar test case, which was not considered in the previous study.

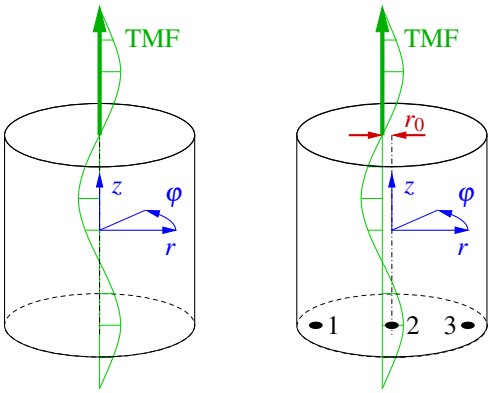

Figure 1. Positioning of the cylindrical container inside the magnetic field in the axisymmetric case (left) and in the case, where the container is shifted by a small offset r_0 (right). The tags 1, 2, and 3 label three different positions on which velocity profiles are compared below.

2 PHYSICAL MODEL

We consider an electrically conducting fluid in a closed cylinder with radius R and height H. The flow is driven by a travelling magnetic field of induction B and angular velocity ω, that generates the upwards driving Lorentz force (cf. Fig. 1). Assuming low-frequency / low-induction and low-interaction conditions, the driving magnetic field decouples from the fluid flow. The Lorentz force $\vec{f}_\mathrm{L}$ can be determined independently as well as the oscillating part of the electromagnetic body force can be neglected [6, 7]. Hence, the flow is governed by the incompressible Navier-Stokes equations including a spatially varying body force.

In the ideal case, where the axes of the magnetic field and the cylinder are perfectly aligned, the Lorentz force is given by the simple expression [2]

$$\vec{f}_\mathrm{L} = \frac{\rho\nu^2}{R^3}\frac{\mathrm{F}}{2} r^2\,\vec{e}_z \tag{1}$$

where $\vec{e}_z$ represents the unit vector in axial direction and F the non-dimensional forcing parameter

$$\mathrm{F} = \frac{\sigma\omega k B^2 R^5}{4\rho\nu^2} \tag{2}$$

with the fluid's density ρ, kinematic viscosity ν, and electrical conductivity σ. The wave number k of the magnetic field is assumed to be large in comparison to the height of the cylinder (for the case of arbitrary wave lengths cf. [1]).

The presence of a small offset r_0 induces an additional forcing $\vec{f}_D$ in form of a vortex (Fig. 2, right), that is comparatively small in comparison to the complete body force (Fig. 2, left). In case of $r_0 = R/30$ the difference to the ideal case accounts for ca. 4 %. Although an axial alignment introduces a higher complexity, the resulting Lorentz force can still be computed analytically (see [5] for further details) and reads:

$$\vec{f}_\mathrm{L} = \frac{\rho\nu^2}{R^3}\frac{\mathrm{F}}{2}\begin{pmatrix} g_z \\ g_r \\ g_\varphi \end{pmatrix} \tag{3}$$

where the shape functions g_z, g_r and g_φ are given by

$$\begin{aligned}
g_z &= \left(\frac{r}{R}\right)^2 + \left[2 - \frac{I_0(kr) - I_2(kr)}{2I_1'(k)}\right]\frac{r}{R}\frac{r_0}{R}cos\varphi \\
&\quad - \frac{r_0}{R}\frac{1}{I_1'(kR)}\left[\hat{j}^1_\varphi \frac{r}{R}\cos(kz) - \hat{j}^2_\varphi \frac{r}{R}\sin(kz)\right] \\
g_r &= -\frac{r_0}{R}\frac{1}{I_1'(kR)}\left[\hat{j}^2_\varphi \frac{2}{kR}\cos(kz) + \hat{j}^1_\varphi \frac{2}{kR}\sin(kz)\right] \\
g_\varphi &= -\frac{r_0}{R}\frac{1}{I_1'(kR)}\left[\left(-\hat{j}^2_r \frac{2}{kR} - \hat{j}^1_z \frac{r}{R}\right)\cos(kz)\right. \\
&\quad \left. + \left(-\hat{j}^1_r \frac{2}{kR} + \hat{j}^2_z \frac{r}{R}\right)\sin(kz)\right]
\end{aligned}$$

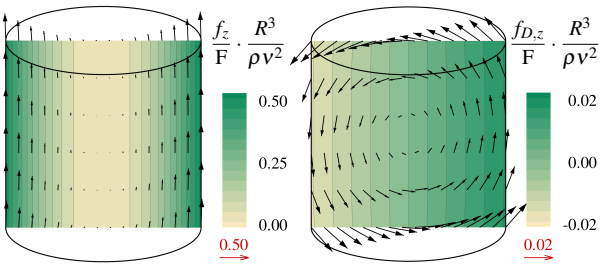

Figure 2. Axial component of the complete Lorentz force $\vec{f}$ (left) and the difference $\vec{f}_D$ from the ideal case (right) for an misalignment of $r_0 = R/30$ and an aspect ratio of $H/2R = 1$.

with the non-dimensional amplitudes of the current density

$$\begin{aligned}
\hat{j}^1_z &= \sin\varphi \sum_{n=1}^{\infty} c_n a_n \sinh\left(\lambda_n \frac{z}{R}\right) J_1\left(\lambda_n \frac{r}{R}\right) \\
\hat{j}^1_r &= \sin\varphi \sum_{n=1}^{\infty} \frac{c_n a_n}{2} \cosh\left(\lambda_n \frac{z}{R}\right)\left[J_0\left(\lambda_n \frac{r}{R}\right) - J_2\left(\lambda_n \frac{r}{R}\right)\right] \\
\hat{j}^1_\varphi &= \cos\varphi \sum_{n=1}^{\infty} \frac{c_n a_n}{2} \cosh\left(\lambda_n \frac{z}{R}\right)\left[J_0\left(\lambda_n \frac{r}{R}\right) + J_2\left(\lambda_n \frac{r}{R}\right)\right] \\
\hat{j}^2_z &= \sin\varphi \sum_{n=1}^{\infty} c_n b_n \cosh\left(\lambda_n \frac{z}{R}\right) J_1\left(\lambda_n \frac{r}{R}\right) \\
\hat{j}^2_r &= \sin\varphi \sum_{n=1}^{\infty} \frac{c_n b_n}{2} \sinh\left(\lambda_n \frac{z}{R}\right)\left[J_0\left(\lambda_n \frac{r}{R}\right) - J_2\left(\lambda_n \frac{r}{R}\right)\right] \\
\hat{j}^2_\varphi &= \cos\varphi \sum_{n=1}^{\infty} \frac{c_n b_n}{2} \sinh\left(\lambda_n \frac{z}{R}\right)\left[J_0\left(\lambda_n \frac{r}{R}\right) + J_2\left(\lambda_n \frac{r}{R}\right)\right]
\end{aligned}$$

and the coefficients

$$\begin{aligned}
a_n &= \frac{\sin(hkR)}{\sinh(\lambda_n h)}, \quad b_n = \frac{\cos(hkR)}{\cosh(\lambda_n h)}, \\
c_n &= \frac{2\lambda_n^2}{R^2(\lambda_n^2 - 1)J_1^2(\lambda_n)} \int_0^R r I_1(kr) J_1\left(\lambda_n \frac{r}{R}\right) \mathrm{d}r .
\end{aligned}$$

Here, J_k and I_k are the Bessel functions and the modified Bessel functions of the k-th kind and λ_n the roots of J_1'.

For the following numerical study two different forcing parameters are considered $\mathrm{F} = 10^5$ and $\mathrm{F} = 10^6$. These values correspond to a slightly subcritical and an eight-times supercritical forcing with regard to the threshold $\mathrm{F}_c = 120{,}400$ [2].

3 NUMERICAL METHOD

As described in the previous section, the flow is governed by the incompressible Navier-Stokes equations

$$\partial_t \vec{u} + \vec{u}\cdot\nabla\vec{u} = -\frac{1}{\rho}\nabla p + \nu\nabla^2\vec{u} + \frac{1}{\rho}\vec{f}_\mathrm{L}\,, \quad \nabla\cdot\vec{u} = 0\,, \tag{4}$$

where $\vec{u}$ and p represent the velocity and the pressure field, respectively. No-slip conditions are applied at the walls. The equations are evaluated in cylindrical coordinates. This allows the application of an efficient spectral element / Fourier method [8], which employs quadrilateral nodal elements in the meridional semi-planes coupled with trigonometric expansions in the azimuth. Time integration is based on the second-order splitting method reported in [9, 10].

For the subcritical test case, i, e. $\mathrm{F} = 10^5$, the computational domain is discretized using 20×10 spectral elements with polynomial order P of 7 and 24 Fourier modes, corresponding to 48 meridional semi-planes. In viscous units, the grid resolution varies from $\delta^+ < 0.2$ near the walls to $\delta^+ < 1.8$ in the core region and ensures fully-resolved (direct) numerical simulations (DNS).

In case of $\mathrm{F} = 10^6$, large-eddy simulations (LES) are performed. As subgrid scale model the spectral vanishing viscosity (SVV) technique is used. This technique was introduced

as a concept for stabilizing Fourier spectral approximations of hyperbolic conservation laws [11]. The idea behind SVV is to define a spectral viscosity that reaches a maximum at high wave numbers, but vanishes completely for wave numbers below a resolution-dependent threshold. Details about the implementation of SVV for axisymmetric configurations are discussed in [12]. In that reference, it is further shown that an LES discretization with 10×5 spectral elements ($P = 7$) and 24 Fourier modes provides a very good agreement with DNS results in case of $\mathrm{F} = 10^6$ and $r_0 = 0$, i. e. perfect alignment. Here, the resolution varies from $\delta^+ < 0.3$ near the walls to $\delta^+ < 4.5$ in the core region. The optimal SVV parameterization, which was determined in that study, is used in the following to examine the influence of an axial misalignment to the fluid properties.

4 RESULTS

For the following investigations, a cylinder with aspect ratio $H/2R = 1$ with $R = 30\,\mathrm{mm}$ is considered, which corresponds to the experimental setup in [5]. Furthermore, the fluid properties of the eutectic alloy gallium-indium-tin (GaInSn) are assumed. This metal has a melting point of 10 °C and, consequently, it is liquid at room temperature. This characteristics allows an easy manageability in experiments and was therefore chosen in [5]. The viscosity, electrical conductivity, and density of GaInSn are given by $\nu = 3.4 \cdot 10^{-7}\,\mathrm{m^2/s}$, $\sigma = 3.3 \cdot 10^6\,\mathrm{S/m}$, and $\rho = 6361\,\mathrm{kg/m^2}$, respectively.

First, we investigate the laminar test case with $\mathrm{F} = 10^5$. The offset r_0 varies between 0 and 1 mm. Thus, the overall deviation of the Lorentz force from the ideal case is at maximum 4 percent (cf. Fig. 2). Figure 3 presents the evolution of the axial velocity profiles in dependence of the offset r_0 along the tag lines 1, 2, and 3. Additionally, the mean flow is illustrated for $r_0 = 0$ and 1 mm in Fig. 4. In the ideal case, the torodial flow is symmetric with regard to the cylinder's axis. When a small displacement is introduced, the upward facing near wall jet at the right side, where the TMF is stronger, becomes more dominant (Fig. 4). Along the corresponding tag line 3, the velocity increases over a wide range (Fig. 3). On the other side of the cylinder, the size of the jet decreases. However, the velocities still have the same order of magnitude as in the unshifted configuration.

Figures 5 and 6 presents the flow characteristics for the

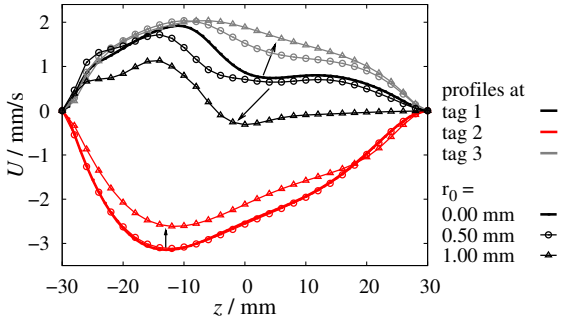

Figure 3. $\mathrm{F} = 10^5$: Profiles of the mean axial velocity U at the tags 1, 2, and 3 in dependence of the offset ($r_0 = 0$, 0.5 and 1 mm).

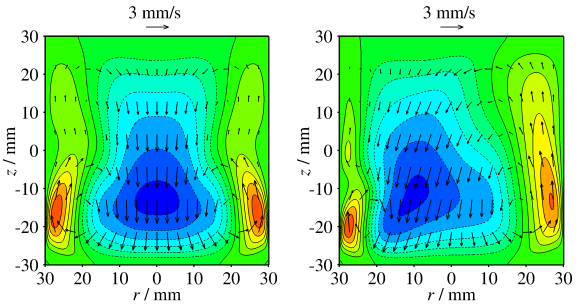

Figure 4. $\mathrm{F} = 10^5$: Mean flow in the frontal section plane (spanned by the tags 1 till 3, cf. Fig. 1) for the axisymmetric case (left) and for an offset of $r_0 = 1\,\mathrm{mm}$ (right). The colour indicates the axial velocity component; contours vary from -3 till 3 mm/s step 0.5 mm/s.

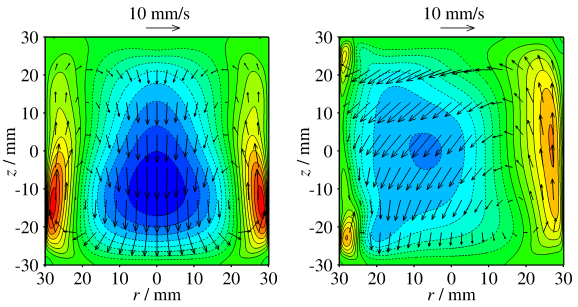

Figure 5. $\mathrm{F} = 10^6$: Mean flow in the frontal section plane for the axissymmetric case (left) and for an offset of $r_0 = 1\,\mathrm{mm}$ (right). Contours of the axial velocity vary from -8 till 8 mm/s step 1 mm/s.

turbulent regime at $\mathrm{F} = 10^6$. As above, displacements with up to $r_0 = 1\,\mathrm{mm}$ are examined. Since the Lorentz force scales linearly with r_0 and independently of the forcing parameter F, the difference from ideal force is at maximum 4 percent in this test case, too. However, the effect to the fluid flow is remarkable. The left upward velocity jet of mean flow vanishes almost completely, only two relicts in the corners are left over (Fig. 5), so that the typical torus structure does not exist anymore. Not only that the symmetry of the mean flow is broken, but also the maximum of the axial velocity is reduced by about 30 % compared to the ideal configuration (Fig. 5). A closer look the development of the velocity profiles in Fig. 6 reveals that this change of the flow patterns does not proceed lineary with increasing r_0. The difference between the profiles for $r_0 = 0.5$ and 1 mm is comparably small in contrast to the changes from 0 to 0.25 mm or from 0.25 to 0.5 mm. Besides the mean flow, the turbulence characteristics changes significantly. Fig. 7 shows a typical vortex distribution for the ideal, perfectly aligned configuration as well as for the simulation with an offset of $r_0 = 1\,\mathrm{mm}$. In both cases, the vortices are visualized with the λ_2 criterium according to [13] using the same λ_2 value. In the ideal case, the vortices cover the whole domain and show a rather random orientation. However, the evolution over a time-span reveals a preference to axial orientation in the centre [4]. In the misaligned configuration, two facts are evident. First, a large horizontal vortex

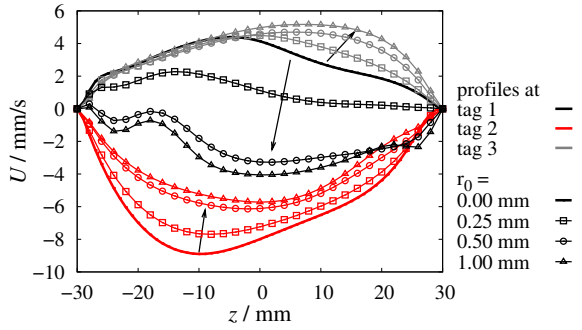

Figure 6. $F = 10^6$: Profiles of the mean axial velocity U at the tags 1, 2, and 3 in dependence of the offset ($r_0 = 0$, 0.25, 0.5 and 1 mm).

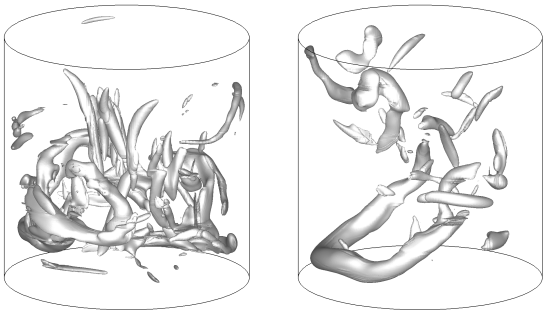

Figure 7. Typical vortex distribution in the axisymmetric (left) and the misaligned configuration with $r_0 = 1$ mm (right).

arises and dominates most of the time the vortex distribution (Fig. 7, right). This structure correlates with the relict of the near-wall jet in the left corner of Fig. 5 (right). Secondly, the amount and the size of the vortices in the rest of the cylinder decreases, when both axes are misaligned. The maximal turbulent kinetic energy decreases by ca. 15 percent in case of $r_0 = 1$ mm.

5 CONCLUSIONS

The study presented in this paper showed that a flow driven by a travelling magnetic field is quite sensitive to small displacements of the container within the magnetic field. In the laminar test case, an offset between the axes of the cylinder and the magnetic field mainly generates a squeeze of the torus structure, but the velocity magnitudes remain comparable to the perfectly aligned configuration. In contrast, the flow structures change remarkably in a turbulent regime. The torus-like mean flow is destroyed even for small offsets and the velocity's magnitudes diminish up to 30 percent. Furthermore, the overall turbulence degree decreases and a single azimuthally orientated vortex prevails the flow in the lower part of the cylinder. In summary, one can conclude that the application of the travelling magnetic field in experimental setups and even more in industrial processes needs an enhanced care in order to cope with the described sensitivity of the flow.

6 ACKNOWLEDGEMENTS

We thank "Deutsche Forschungsgemeinschaft" for financial support in the framework of the Collaborative Research Centre SFB 609 and H.M. Blackburn for providing the flow solver *Semtex*. The computations were performed on an SGI Altix system based on a grant from the Center for Information Services and High Performance Computing (ZIH) at TU Dresden.

REFERENCES

[1] N. Ramachandran, K. Mazuruk, and M. P. Volz, "Use of traveling magnetic fields to control melt convection," *J. Jpn. Soc. Microgravity Appl.*, vol. 17, no. 2, pp. 98–103, 2000.

[2] I. Grants and G. Gerbeth, "Stability of melt flow due to a traveling magnetic field in a closed ampoule," *J. Cryst. Growth*, vol. 269, pp. 630–638, 2004.

[3] A. Cramer, J. Pal, and G. Gerbeth, "Experimental investigation of a flow driven by a combination of a rotating and a traveling magnetic field," *Phys. Fluids*, vol. 19, p. 118109, 2007.

[4] J. Stiller and K. Koal, "A numerical study of the turbulent flow driven by rotating and travelling magnetic fields in a cylindrical cavity," *J. Turbulence*, vol. 10, no. 44, pp. 1–16, 2010.

[5] A. Cramer, J. Pal, K. Koal, S. Tschisgale, J. Stiller, and G. Gerbeth, "The sensitivity of a travelling magnetic field driven flow to axial alignment," *J. Cryst. Growth, in press*, 2011.

[6] P. A. Davidson and J. C. R. Hunt, "Swirling recirculating flow in a liquid-metal column generated by a rotating magnetic field," *J. Fluid Mech.*, vol. 185, pp. 67–106, 1987.

[7] L. Martin Witkowski, J. S. Walker, and P. Marty, "Non-axisymmetric flow in a finite-length cylinder with a rotating magnetic field," *Phys. Fluids*, vol. 11, no. 7, pp. 1821–1826, 1999.

[8] H. M. Blackburn and S. Sherwin, "Formulation of a Galerkin spectral element-Fourier method for three-dimensional incompressible flows in cylindrical geometries," *J. Comp. Phys.*, vol. 197, pp. 759–778, 2004.

[9] G. Karniadakis and S. Sherwin, *Spectral/hp Element Method for CFD*. Oxford University Press, 1999.

[10] J. L. Guermond, P. Minev, and J. Shen, "An overview of projection methods for incompressible flows," *Comput. Methods Appl. Mech. Engrg.*, vol. 195, pp. 6011–6045, 2006.

[11] E. Tadmor, "Convergence of spectral methods for nonlinear conservation laws," *SIAM J. Numer. Anal.*, vol. 26, no. 1, pp. 30–44, 1989.

[12] K. Koal, J. Stiller, and H. M. Blackburn, "Adapting the spectral vanishing viscosity method for large-eddy simulations in cylindrical configurations," *submitted to J. Comp. Phys.*, 2011.

[13] J. Jeong and F. Hussain, "On the identification of a vortex," *J. Fluid Mech.*, vol. 285, pp. 69–94, 1995.